Nonlinear development of flow patterns in an annulus with decelerating inner cylinder

Takashi Watanabe[a)]
Center for Information Media Studies, Nagoya University, Furu-cho Chikusa-ku Nagoya, 464-8603 Japan

Hiroyuki Furukawa[b)]
Graduate School of Human Informatics, Nagoya University, Furo-cho Chikusa-ku Nagoya, 464-8601 Japan

Ikuo Nakamura[c)]
Department of Mechanical Engineering, Meijo University, 1-501 Shiogamaguchi Tempaku-ku Nagoya, 468-8502 Japan

(Received 21 February 2001; accepted 28 August 2001)

Decelerating Taylor vortex flow between two concentric cylinders is investigated by using the time-dependent numerical method. The lengths of the rotating inner cylinder and the stationary outer cylinder are finite. We focus on the mode transitions from well-developed flows during the gradual decrease in the angular velocity of the inner cylinder. In the range of the Reynolds number from 50 to 1000 and the range of the aspect ratio Γ from 2.6 to 7.2, the exchanges of flow pattern from normal secondary modes to primary modes are clarified, and the Reynolds numbers at which the flow modes exchange are determined. The reduction of the number of cells in the flow of the normal mode begins with the weakening of a pair of counter-rotating cells with an inward radial flow at their boundary. An anomalous cell has two extra cells at corners of the end wall and the cylinder walls. In the transient process from the flow of the anomalous mode, extra cells grow and merge into a normal cell, and a saddle point appears in the working fluid. As the merged cell enlarges, the saddle point vanishes and the global normal flow mode appears. The result shows good agreement with experimental observations.
[DOI: 10.1063/1.1416498]

I. INTRODUCTION

Although Taylor vortex flow developing between two concentric rotating cylinders is a classical flow, it has attracted great attention as a typical problem in nonlinear dynamics. In the case of high Reynolds numbers, the onset of wavy Taylor vortex flows and the transition to chaotic flows have been examined.[1–3] When the Reynolds number is low and the lengths of cylinders are finite, various flow patterns appear.[4,5]

In the seminal studies of Benjamin[4] and Benjamin and Mullin,[6] Taylor vortex flows between two cylinders with finite length are classified into some modes as shown in Fig. 1.[7] At a constant aspect ratio, the flow is classified as a primary mode and secondary modes. The primary mode flow is formed smoothly from Couette flow by a gradual increase in the Reynolds number. The secondary mode appears when the Reynolds number is increased abruptly until around a certain value. The number of vortices in the secondary mode is different from one in the primary mode. The primary mode and secondary mode are distinguished into a normal mode and an anomalous mode. On each end wall, the flow in the normal mode has a normal cell which gives an inward flow in the region adjacent to the end wall. The flow of the anomalous mode has an anomalous cell which gives an outward flow near the end wall. Now, this mode classification is a *de facto* standard, and many numerical investigations have been carried out on the mode formation. Cliffe *et al.*[8] and Anson and Cliffe[9] introduced Schaeffer's homotopy parameter in order to estimate the influence of the end walls of the cylinders. Their numerical and experimental results showed an anomalous mode with an outward flow near the end wall. Bolstad and Keller[10] also adopted Schaeffer's model and obtained five distinct solutions at a fixed Reynolds number, aspect ratio and radius ratio. The Reynolds number Re is based on the rotation speed of the inner cylinder and the aspect ratio Γ is the ratio of the cylinder length to the gap width between cylinders. The radius ratio η is the ratio of the radius of the inner cylinder to the one of the outer cylinder. They claimed that, even in the flow of an anomalous mode, a hidden vortex which was not observed by a usual visualization appeared and the flow was not at all outward in the region adjacent to the end wall. In contrast to their conclusion, the experiment of Nakamura and Toya[7] clearly showed the outward flow on the end wall.

Cliffe[11] adopted the steady equations and determined the bifurcation loci between the two-cell primary mode and four-cell secondary mode and the loci between the four-cell primary mode and six-cell secondary mode in the (Re,Γ) plane. They found that, for a certain range of the aspect ratio, the six-cell secondary mode loses its stability to asymmetric dis-

a)Electronic mail: watanabe@info.human.nagoya-u.ac.jp
b)Electronic mail: hiroyuki@info.human.nagoya-u.ac.jp
c)Electronic mail: inakamu@meijo-u.ac.jp

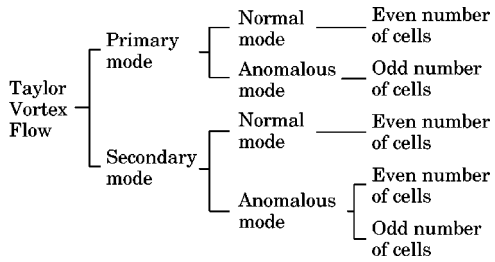

FIG. 1. Classification of Taylor vortex flow. Cylinder length is finite and both end walls are stationary.

turbances. Pfister *et al.*[12] used the unsteady equations and found a symmetric two-cell mode and a single-cell mode. They determined boundaries separating regions where flows of these modes appear. The unsteady flow calculation carried out by Ball and Farouk[13] showed the regions of the two-cell, four-cell, and six-cell modes. Hirshfeld and Rapaport[14] assumed the axial periodicity and obtained a flow developing from rest, via intermediate five-cell mode, to the normal four-cell mode. In these studies, the main focus was the modes of the fully developed flow, and the mode transition process was not discussed.

Even when the Reynolds number is less than the critical value at which steady Taylor cells arise, Ekman vortices develop on stationary end walls of an annulus with finite length.[15] Lücke *et al.*[16] studied the time-dependent case in which the rotation speed of the inner cylinder was suddenly increased from zero and examined the propagation of the end-wall effect into the entire region. Neitzel[17] assumed that the end walls started to rotate impulsively together with the inner cylinder. He found that Taylor cells were generated and merged with each other during the developing process, and the final mode appeared after a reduction of the number of cells. Flows with a gradual increase in the Reynolds number were computed by Kuo and Ball,[15] and an evolution of series of vortices from end walls was clarified. Takeda *et al.*[18] investigated these unsteady phenomena experimentally, and showed no evidence that Taylor cells were induced by Ekman vortices on end walls.

When the Reynolds number gradually decreases, the secondary mode flow is attracted to the primary mode flow. Benjamin and Mullin,[6] for example, examined these phenomena experimentally and discriminated the range of the Reynolds number in which the mode changes. Nakamura *et al.*[19] carried out experimental investigations and showed bifurcation processes from the secondary modes, occasionally via other secondary modes, to the primary modes. Bieleck and Koschmieder[20] counted the number of vortices which emerged after sudden starts of the inner cylinder with moderate aspect ratios. They observed the increase and decrease of the number of vortices when the Reynolds number is decreased.

There are only a few studies on numerical studies on decelerating Taylor flows. Alziary de Roquefort and Grillaud[21] investigated the stepwise decelerating flows, and Hirshfeld and Rapaport[22] used a molecular dynamics method and calculated flows with a sudden start or stop. However, these results did not reveal any mode exchanges. Hill[23] predicted the mode transition which was found by Benjamin and Mullin,[6] but the case was limited only to the exchange between the four-cell mode and six-cell mode. Barenghi[24] and Streett and Hussaini[25] presented the mode exchange from the normal secondary two-cell mode to the primary four-cell mode with a gradual increase in the Reynolds number. They described, however, few comments about the detail of the collapse of vortices.

Today, the transient dynamics is one of hot topics of the nonlinear dynamics,[26] where the research target is not only the asymptotic state of the phenomena but also the time-developing behaviors of the solution in the global spatial domain. The result of the flow visualization[19] has clarified that the onset processes of Taylor vortex flow show transitions of entire flow patterns, and the pattern exchanges are interesting to be regarded as transient dynamics. However, no numerical study known to the authors aims at the pattern transition.

In this study, we conduct a numerical investigation on the mode exchange processes of flows between a rotating inner cylinder and a stationary outer cylinder, and unveil the mode formation processes which are difficult to be observed in experiments. For the range of the Reynolds number from 50 to 1000 and the range of the aspect ratio from 2.6 to 7.2, the unsteady mode transitions from the secondary modes to the primary modes are examined, and the numerical results are compared with experimental results.

In the rest of the paper, Sec. II contains a description of the numerical method used in this study and Sec. III presents the numerical results and discussions. Finally, Sec. IV concludes this paper.

II. NUMERICAL METHOD

Flows between two concentric cylinders are considered. The lengths of the cylinders are finite, and the end walls of the cylinders are stationary solid walls. The outer cylinder is fixed and the inner cylinder rotates. All physical parameters are scaled by the characteristic length which is the gap width between the radii of cylinders, the characteristic velocity which is the maximum circumferential velocity attained during each calculation run and the characteristic time defined as the ratio of the characteristic length to the characteristic velocity. Dimensionless radii of the inner and outer cylinders are r_i and r_0, respectively, and the length of cylinders is l. The gap between cylinders is indicated by $d(=1)$, and the aspect ratio Γ is given by l/d. The Reynolds number based on the characteristic velocity is denoted by Re_0, and the Reynolds number based on an instantaneous rotation velocity of the inner cylinder is Re. The governing equations are the unsteady axisymmetric Navier–Stokes equations and the equation of continuity expressed in the cylindrical coordinate system (r,θ,z) which is suitable for the present calculation:

$$r: \frac{\partial u}{\partial t}+u\frac{\partial u}{\partial r}+w\frac{\partial u}{\partial z}-\frac{v^2}{r} = -\frac{\partial p}{\partial r}+\frac{1}{\mathrm{Re}_0}\left(\frac{\partial^2 u}{\partial r^2}+\frac{1}{r}\frac{\partial u}{\partial r}-\frac{u}{r^2}+\frac{\partial^2 u}{\partial z^2}\right), \quad (1)$$

$$\theta: \frac{\partial v}{\partial t}+u\frac{\partial v}{\partial r}+w\frac{\partial v}{\partial z}+\frac{uv}{r} = \frac{1}{\mathrm{Re}_0}\left(\frac{\partial^2 v}{\partial r^2}+\frac{1}{r}\frac{\partial v}{\partial r}-\frac{v}{r^2}+\frac{\partial^2 v}{\partial z^2}\right), \tag{2}$$

$$z: \frac{\partial w}{\partial t}+u\frac{\partial w}{\partial r}+w\frac{\partial w}{\partial z} = -\frac{\partial p}{\partial z}+\frac{1}{\mathrm{Re}_0}\left(\frac{\partial^2 w}{\partial r^2}+\frac{1}{r}\frac{\partial w}{\partial r}+\frac{\partial^2 w}{\partial z^2}\right), \tag{3}$$

$$\frac{1}{r}\frac{\partial (ru)}{\partial r}+\frac{\partial w}{\partial z}=0, \tag{4}$$

where t is time, (u,v,w) is the velocity components in the directions of (r,θ,z) and p is the pressure. The radial rate of strain on the inner and outer cylinder walls, and the circumferential rate of strain on the lower and upper cylinder end walls are

$$r\frac{\partial (v/r)}{\partial r}\bigg|_{r=r_i,r_0}, \tag{5}$$

$$\frac{\partial u}{\partial z}\bigg|_{z=z_l,z_u}, \tag{6}$$

where z_l and z_u denote the axial positions of the lower and upper end walls, respectively. Equations (5) and (6) correspond to wall shear stresses, which can be parameters sensitive to the vortex structure. The Stokes' stream function ψ is given by

$$u=-\frac{1}{r}\frac{\partial \psi}{\partial z}, \quad w=\frac{1}{r}\frac{\partial \psi}{\partial r}. \tag{7}$$

The basic solution procedure is the marker-and-cell method. The time integration is the Euler explicit method, and the spatial differentiation is the QUICK method for the convection terms and the second-order central difference method for other terms.[27] The Poisson equation for the pressure is

$$\frac{\partial^2 p}{\partial r^2}+\frac{1}{r}\frac{\partial p}{\partial r}+\frac{\partial^2 p}{\partial z^2} = -\left(\frac{\partial u}{\partial r}\frac{\partial u}{\partial r}+\frac{\partial w}{\partial z}\frac{\partial w}{\partial z}+2\frac{\partial u}{\partial z}\frac{\partial w}{\partial r} +2\frac{1}{r}\frac{\partial v}{\partial z}-2\frac{v}{r}\frac{\partial v}{\partial r}+\frac{u^2}{r^2}\right)-\frac{\partial D}{\partial t}, \tag{8}$$

where D is the divergence of the velocity vector. A hybrid method of SOR and ILUCGS is used to solve the Poisson equation.

The boundary conditions for the velocity components are

$$\begin{aligned} &\text{inner cylinder:} \quad u=w=0, \ v=r_i\omega, \\ &\text{outer cylinder, end walls:} \quad u=v=w=0, \end{aligned} \tag{9}$$

where ω is the angular velocity of the inner cylinder. The boundary condition for the pressure is a Neumann condition estimated from the momentum equations. The initial conditions are evaluated by assuming Couette flow, although this assumption is not valid near the end walls of cylinders.

The staggered grid is adopted and the grid interval is uniform in each direction. Although the corner between the inner cylinder wall and end wall of the cylinder is a singular point, the staggered grid eliminates the difficulty in locating the velocity and pressure components on the singular point. The number of grid points in the radial direction is 41, and the number of grid points in the axial direction is determined by the proportionality to the cylinder length with 42 points for a unit aspect ratio. Even though the grids were refined by halving the spacing in each direction or the fourth-order Runge–Kutta method was adopted for the time integral, no observable difference was found in the result. This ensures that the number of grid points used in the present calculation is large enough not to exert observable influence on results. The time step Δt is specified by the relationship $\Delta t/\mathrm{Re}_0 = 1.2\times 10^{-5}$ by which the Courant condition for stability is ensured. The convergence criterion of the iterative method for the pressure Poisson equation is $e_{\mathrm{res}}<10^{-8}$, where e_{res} is the relative residual sum of squares.

In the present calculation, a fully developed flow at a certain Reynolds number is established for a fixed value of the aspect ratio, and then the Reynolds number is gradually decreased in order to investigate the transitions from the secondary modes to the primary modes. The mode transition of decelerating Taylor flow is investigated experimentally by Nakamura *et al.*[19] The experimental apparatus used by them had an inner cylinder with radius 20 mm and an outer cylinder with radius 30 mm (for details, see Ref. 19). For the comparison with their experimental result, the radius ratio $\eta=r_i/r_0$ is fixed at 0.667. Fully developed flow is assumed to be attained when the relative variation of the torque acting on the inner cylinder remains less than 10^{-4}. For the numerical prediction of decelerating flows, fully developed flows are established by a dimensionless time t_1, and then the Reynolds number decreases linearly during a dimensionless time t_2. The dimensionless times t_1 and t_2 correspond to 50 seconds in dimensional form when they are evaluated by the physical dimensions of the cylinders and the kinematic viscosity of aqueous solution of glycerol (6×10^{-6} m^2/s) used in the Nakamura *et al.* experiment.[19] In the following, for a better intuitive understanding of readers, the z coordinate is normalized not by the characteristic length d but by the length of cylinders l.

III. RESULTS AND DISCUSSIONS

A. Transition from the normal mode

As observed in the previous work,[4] the primary mode appears at low Reynolds numbers. The cell number N of the primary mode is uniquely determined by the aspect ratio. When the Reynolds number is increased abruptly, the normal secondary mode with $N+2$ cells appears. Let Re_1 be the Reynolds number at which the secondary mode with $N+2$ cells appears, and Re_2 be the one at which the primary mode with N cells arises. During the reduction of the Reynolds number from Re_1 to Re_2, mode transitions from the normal

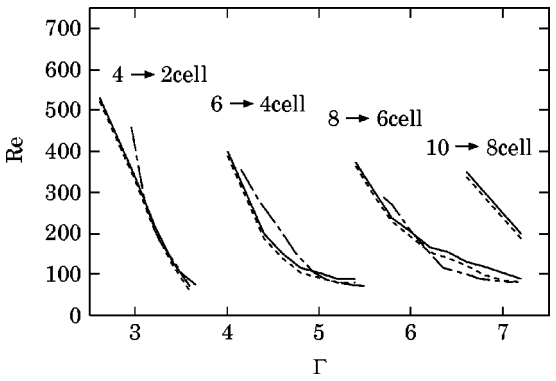

FIG. 2. Bifurcation from normal secondary modes to primary modes. —: lower limit of secondary mode (Re_1). ---: upper limit of primary mode (Re_2). —·—·—·—: experimental result (Ref. 19).

secondary mode to the primary mode occur. Figure 2 shows the bifurcation set in the (Γ,Re) plane. In this figure, the difference between Re_1 and Re_2 is narrowed to about 10 and the deceleration is slowed. The results of the quasisteady experiment by Nakamura *et al.*[19] are also presented. The transitions from the four-cell mode to the two-cell mode at $2.8 \leqslant \Gamma \leqslant 3.6$, from the six-cell mode to the four-cell mode at $4.0 \leqslant \Gamma \leqslant 5.4$ and from the eight-cell mode to the six-cell mode at $5.4 \leqslant \Gamma \leqslant 7.2$ are predicted, and they show good agreement with the experimental results. The transition from the ten-cell mode to the eight-cell mode at $6.6 \leqslant \Gamma \leqslant 7.4$ is not confirmed by the Nakamura *et al.* experiment.[19] Mullin[28] determined the critical loci where the flows change from the ten-cell mode to the eight-cell mode. In his work, the range of the aspect ratio where the mode exchanges occur is about $8.8 \leqslant \Gamma \leqslant 9.5$, which is beyond the scope of our calculations. The critical Reynolds number for the onset of Taylor vortices in an infinite annulus at $\eta = 0.667$ is about 75.[29] Because the critical Reynolds number is not sensitive to the aspect ratio,[30] well-developed Taylor vortex flow is expected to be established at the Reynolds number immediately above the critical value. At Re=75, the primary mode appeared throughout the entire range of the aspect ratios covered in the present study. This result coincides with the experimental observation: the two-cell primary mode at $2.6 \leqslant \Gamma \leqslant 3.6$, four-cell mode at $3.8 \leqslant \Gamma \leqslant 5.4$, and six-cell mode at $5.6 \leqslant \Gamma \leqslant 7.2$. The agreement demonstrates the validity of the present numerical scheme.

In the range of the aspect ratio from 6.6 to 7.2, two different mode transitions appear during the decelerations of the Reynolds numbers. At $\Gamma = 7.0$, for example, one is the transition from the eight-cell mode to the six-cell mode when the Reynolds number is reduced from 105 to 87.5, and the other is the transition from the ten-cell mode to the eight-cell mode observed during the decrease of the Reynolds number from 250 to 240. As the Reynolds number is reduced linearly from 250 to 80, these two mode transitions are observed in succession, and the transition from the normal ten-cell mode, via the normal eight-cell mode, to the normal six-cell mode is confirmed.

The development of flow field from the normal secondary six-cell mode to the primary four-cell mode is shown in

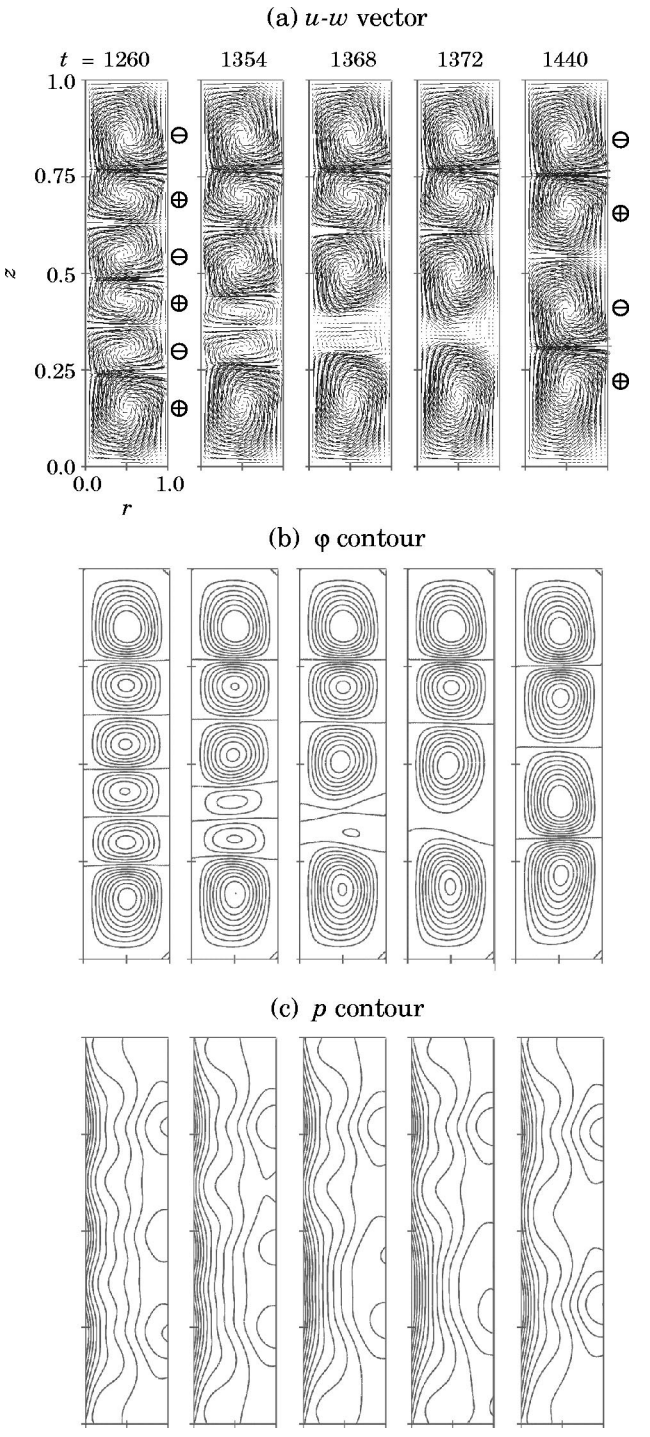

FIG. 3. Development of flow field from normal secondary mode to primary mode. The aspect ratio is 4.6 and the Reynolds number is reduced from 150 to 140. Deceleration starts at $t=450$ and ends at $t=900$.

Figs. 3 and 4. Each figure shows a profile in the meridional section, and the rotating inner cylinder is on the left-hand side and the stationary outer cylinder is on the right-hand side. The aspect ratio is 4.6, and the flow of the secondary mode at Re=150 is fully established at $t=450$. In the following, the calculation conditions which give representative mode transitions are adopted. The reduction of the Reynolds number starts at $t=450$ and ends at $t=900$. After $t=900$, the Reynolds number is kept at a constant value of 140. The

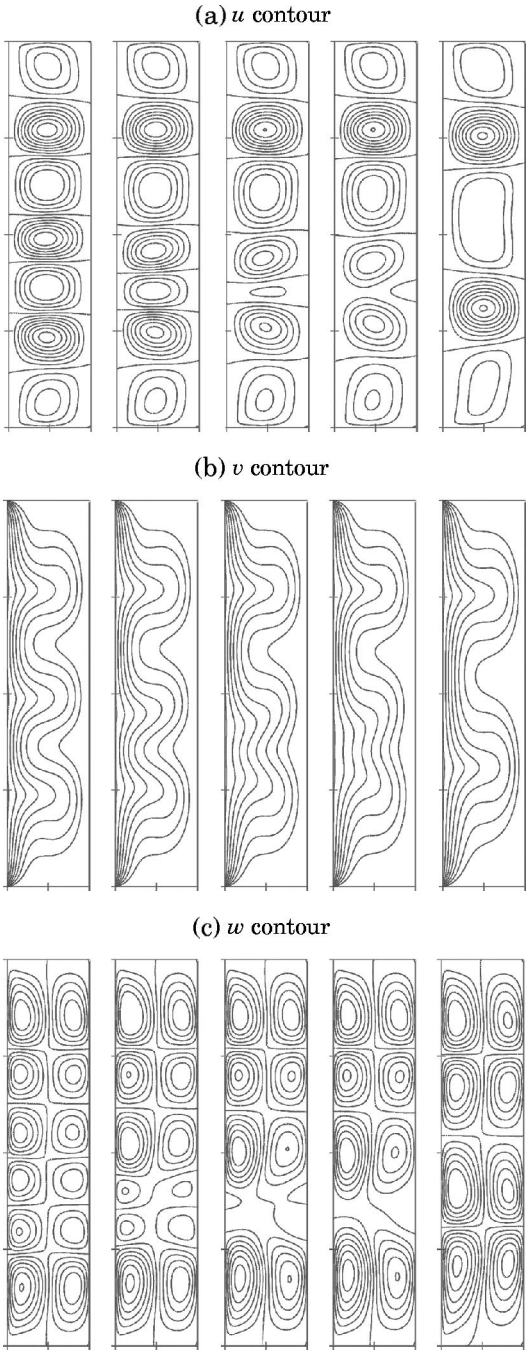

FIG. 4. For caption see Fig. 3.

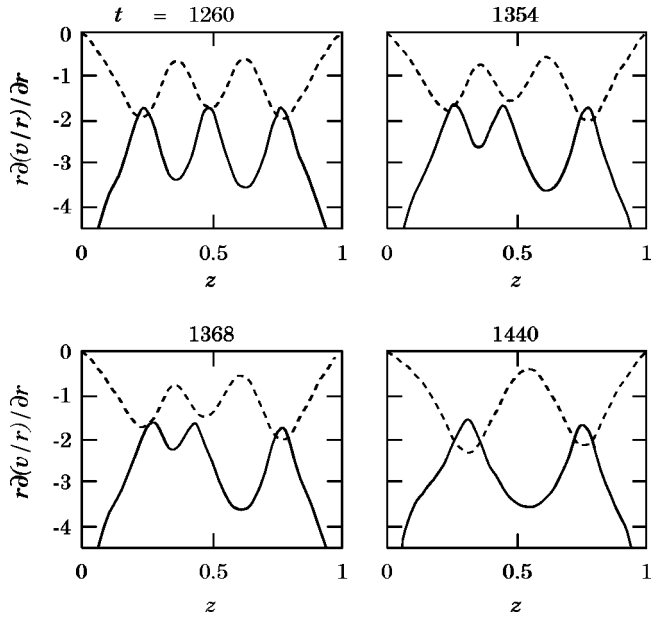

FIG. 5. Variation of circumferential rate of strain on cylinder walls. The aspect ratio is 4.6 and the Reynolds number is reduced from 150 to 140. Deceleration starts at $t=450$ and ends at $t=900$. —:$r=r_i$. ---:$r=r_0$.

mode transition occurs after the deceleration ends at $t=900$. The velocity vector at $t=1260$ and 1440 in Fig. 3(a) are accompanied by plus symbols $\oplus$ which indicate that the rotating direction is clockwise and minus symbols $\ominus$ which indicate that the rotating direction is counterclockwise. Before $t=900$, no appreciable change was observed. The velocity vectors and the contours of the stream function ψ show that a pair of counter-rotating cells, which is around the axial position $z=0.35$, gradually weakens, and the pair is overlapped by the neighboring cells and disappears. The flow at the boundary between the two cells of the pair is inward and the slower fluid flows from the outer cylinder towards the inner cylinder. These results agree with Fig. 4 in the paper of Neitzel[17] who investigated the flow with large aspect ratio. In Fig. 3(c), it is difficult to count the number of cells and to observe the disappearing cells. The contours of the value of u in Fig. 4(a) show that the extrema appear above and below the centers of the cells. The normal six-cell mode has seven extrema of the value of u, and the number of extrema does not correspond with the number of cells. As the flow changes, the third extremum from the lower end wall disappears, and the second extremum and the fourth extremum merge with each other. Finally, five extrema remain even though the flow has four cells. The contours of v in Fig. 4(b) show that the retarded flow propagates to the inner region of the annulus around the axial position where the inward flow occurs. In Fig. 4(c), the pattern of w contours change asymmetrically in the axial direction. As can be seen from this case, the transition phenomenon from a secondary mode with an even number of cells to another mode may not be symmetric with respect to the midplane. The u, v, w, and p contours of fully developed flow are similar to those obtained by Liao *et al.*[2] Bolstad and Keller[10] reported that the flow in an asymmetric steady mode also has a mode whose pattern has a mirror symmetry with respect to the axial direction. In the present study, when the scanning sequence of variables to solve the pressure Poisson equation is reversed, the mirror-imaged flow pattern is obtained.

Components of wall shearing stresses exhibit quantitative aspects of mode exchanges most clearly. The variation of the circumferential rates of strain on cylinder walls is shown in Fig. 5. As the transition proceeds, the absolute value on the inner cylinder wall decreases at about $z=0.35$ where there exists a boundary of disappearing cells and the radial inward flow is observed. The absolute value of the extremum on the outer cylinder, on the other hand, becomes smaller around the midplane where the radial flow is out-

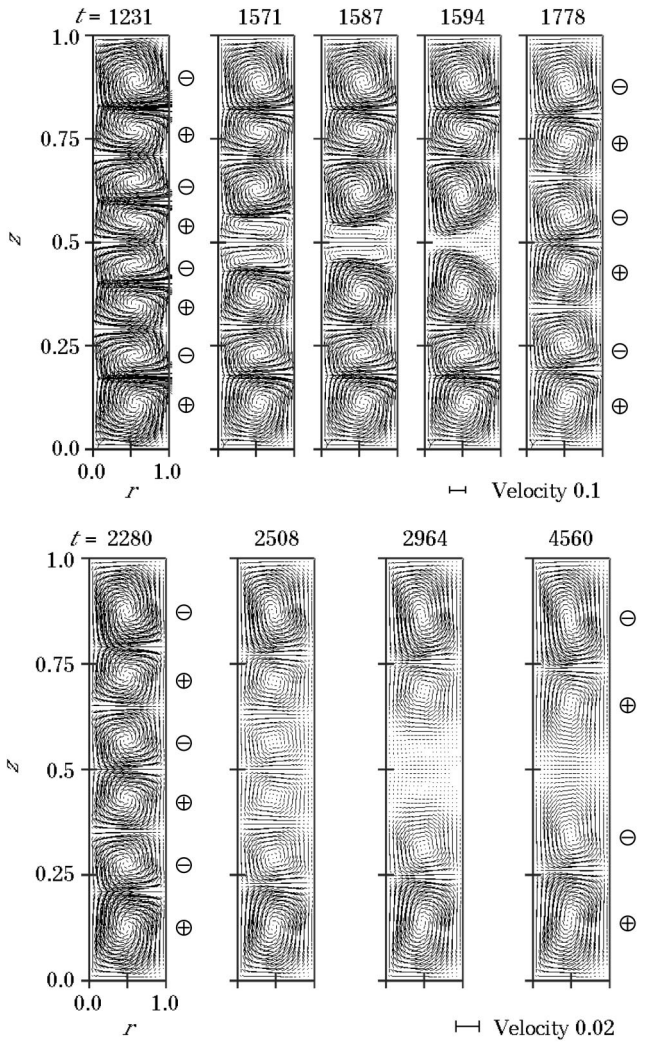

FIG. 6. Development of flow field from normal secondary mode to primary mode. The aspect ratio is 5.4 and the Reynolds number is reduced from 380 to 80. Deceleration starts at $t=1140$ and ends at $t=2280$.

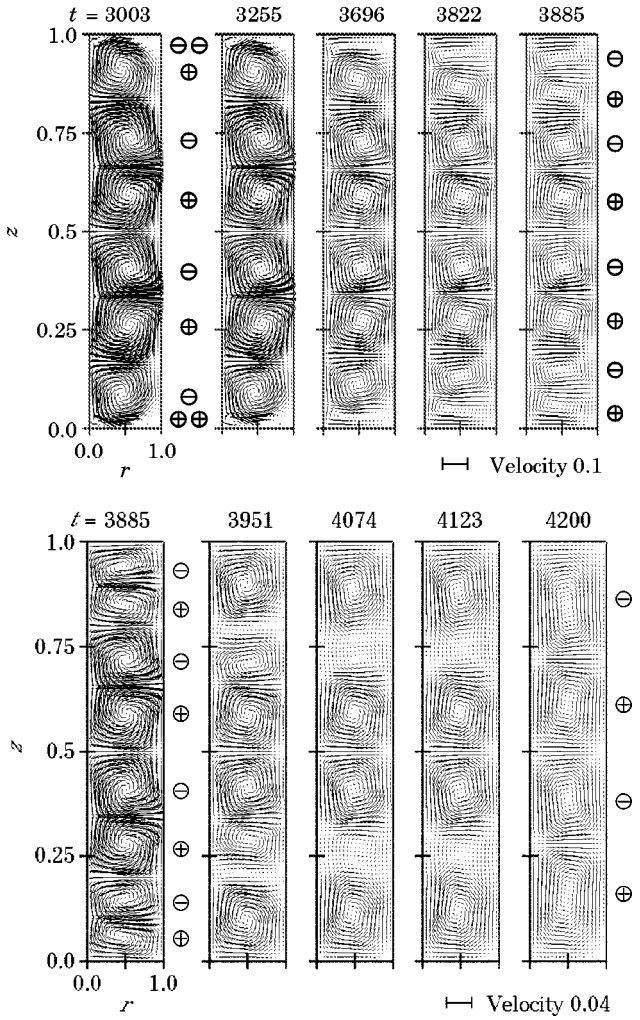

FIG. 7. Development of flow field from secondary anomalous mode to primary mode. The aspect ratio is 5.4 and the Reynolds number is reduced from 700 to 80. Deceleration starts at $t=2100$ and ends at $t=4200$.

ward. After the extremum disappears, the flow mode changes to the primary four-cell mode.

Figure 6 shows the development of the flow field in the case where the aspect ratio is 5.4 and the Reynolds number decreases from 380 to 80. The secondary mode at $\mathrm{Re}=380$ has eight cells. As the Reynolds number decreases, a pair of cells around the midplane collapses and the flow mode changes to the six-cell mode. The pair of disappearing cells has an inward flow at the cells' boundary. Although the six-cell mode remains for a while, it is an intermediate mode. After the termination of the reduction in the Reynolds number, another pair of cells around the midplane decays. Cells on both sides of the pair grow and the flow mode changes to the four-cell mode. The transitions shown in Fig. 6 are almost symmetric in the axial direction.

B. Transition from the anomalous mode

In this section, transformations from anomalous secondary modes to primary modes will be presented, which occur during or after the deceleration of the inner cylinder. The anomalous secondary mode has even or odd number of cells.

Figure 7 shows the variation of velocity vectors at $\Gamma=5.4$. The Reynolds number is decreased from 700 to 80. The primary mode at this aspect ratio has four cells. When the Reynolds number is 700, an anomalous secondary mode with six cells appears. The anomalous mode has two extra cells on the end wall[7] and each has its own extremum value of the stream function: one is on the inner cylinder side, and the other is on the outer cylinder side. The development of extra cells is shown in Fig. 8. At $t=3003$, the extra cells appear on the upper and lower end walls. The boundaries between the anomalous cells and the extra cells reach the end walls. As the Reynolds number decreases, two attached points on the end wall approach each other. They meet around at $r=0.5$ ($t=3255$) and part from the end wall ($t=3339$). Then, a saddle point emerges in the working fluid, and the inner and outer extra cells merge into one vortex ($t=3486$). The saddle point and the outer extremum disappear ($t=3612$) and the merged vortex becomes a normal cell ($t=3696$). After the flow becomes normal, the new normal cell grows as large as other cells, and a pair of cells

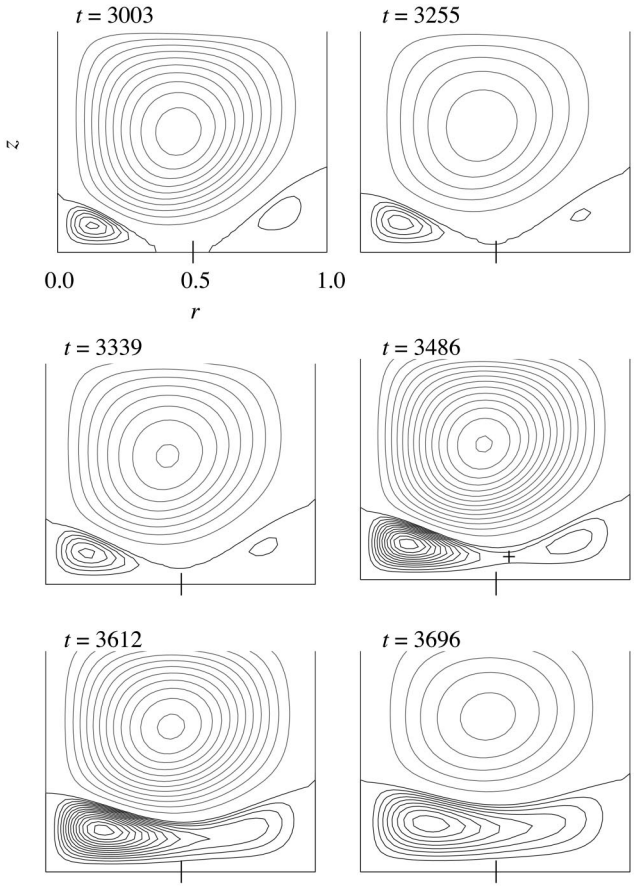

FIG. 8. Variation of contours of stream function ψ around an anomalous cell near the end wall. The aspect ratio is 5.4 and the Reynolds number is reduced from 700 to 80. Deceleration starts at $t=2100$ and ends at $t=4200$. +: saddle point.

which is adjacent to the merged cell becomes weak. The weakening cells have a boundary with an inward flow between them. The mode transition is almost symmetric in the axial direction, and there are two pairs of weakening cells. Finally these pairs vanish, and the flow becomes the primary four-cell mode.

In order to confirm that the saddle point appears in the flow region, the spacial variation of the velocity components near the saddle point at $t=3486$ in Fig. 8 is examined. When the values of the velocity component w are scanned from the inner cylinder to the outer cylinder, they change from negative to positive near the saddle point. Being swept from the lower end wall to the upper end wall, the values of the velocity component u change from negative to positive. This ensures the existence of the saddle point.

An anomalous cell which is originally attached to the end wall is detached from the wall by the growth of extra cells. In order to indicate this evidence more clearly, path lines of the flow in Figs. 7 and 8 are shown in Fig. 9. Initially, the passive particles are captured by the extra cells. As the outer cell extends in the radial direction and covers the inner cell, the particles leave from walls.

In Fig. 10, profiles of the radial component of strain rates on the end walls are presented. At $t=2940$, the positive or negative sign of the strain rate reveals that the flow direction

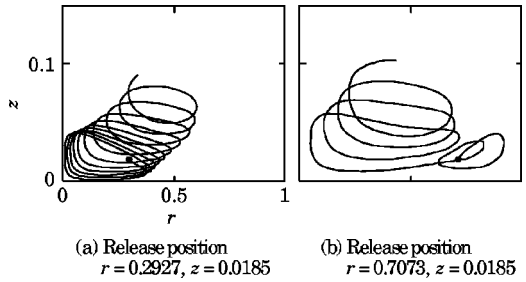

FIG. 9. Path lines of particles released at $t=3234$ and traced until $t=3648$. The aspect ratio is 5.4 and the Reynolds number is reduced from 700 to 80. Deceleration starts at $t=2100$ and ends at $t=4200$. ●: position where a particle released.

is outward on the middle part of the end wall, while the flow direction is inward in regions near the inner and the outer cylinders. As the extra cells grow, the anomalous cell is detached from the end wall and the flow direction becomes inward over the entire region.

Cliffe and Mullin[31] confirmed the anomalous three-, four- and five-cell mode experimentally and numerically. The flow of the anomalous mode has an anomalous cell which gives an outward flow near the end wall. Bolstad and Keller,[10] on the other hand, argued that the flow of the anomalous mode contained a hidden vortex between the anomalous cell and the end wall, and the flow was not at all outward on the end wall. The hidden vortex is thin and it extends from the inner cylinder wall to the outer cylinder wall. In the present study, the existence of an anomalous cell and extra cells in Fig. 8 and the profile of the strain rate in Fig. 10 show that there is a region where the anomalous cell reaches the end wall and the anomalous cell has an outward flow on the end wall. This evidence suggests that the anomalous mode has no hidden vortex whose existence is predicted by Bolstad and Keller. The recent experiments of Nakamura and Toya[7] also confirmed that the anomalous cell has outward flow along the fixed end wall.

Figure 11 shows the transition from the anomalous secondary mode with an odd number of cells. The aspect ratio is 4.4 and the Reynolds number decreases from 600 to 100. Two extra cells are formed on the upper end wall where an anomalous cell appears. The anomalous cell originally attaches to the end wall. As the rotation speed decreases, the

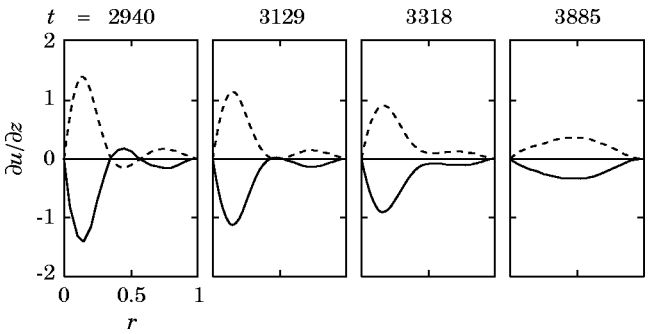

FIG. 10. Variation of radial rate of strain on cylinder end walls. The aspect ratio is 5.4 and the Reynolds number is reduced from 700 to 80. Deceleration starts at $t=2100$ and ends at $t=4200$. —: $z=z_l$. ---: $z=z_u$.

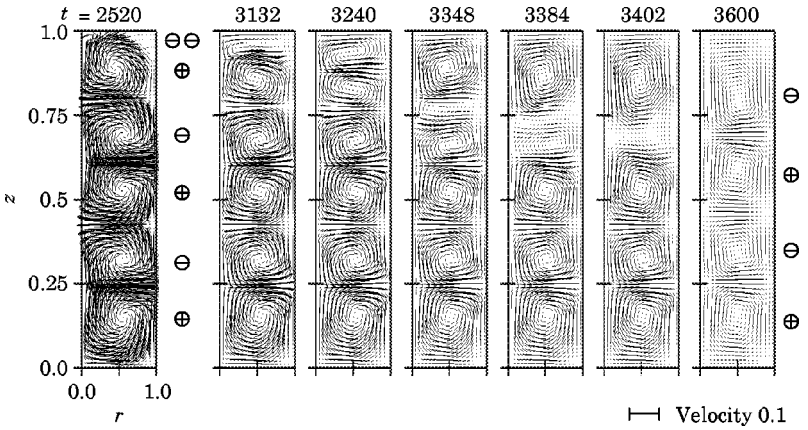

FIG. 11. Development of flow field from secondary anomalous mode to primary mode. The aspect ratio is 4.4 and the Reynolds number is reduced from 600 to 100. Deceleration starts at $t=1800$ and ends at $t=3600$.

extra cells merge into a normal cell, and the flow becomes the normal six-cell mode. While the merged cell grows, a pair of cells adjacent to the merged cell disappears, and the flow changes to the primary four-cell mode.

In the range of the Reynolds number Re from 50 to 1000 and the range of the aspect ratio Γ from 2.6 to 7.2, the various modes with even and odd numbers of cells from 2 to 10 appear. Figure 12 shows the confirmed structures of the partial orders which represent the transition processes in the sense of algebra. The arrows represent the directions of mode exchanges. While a greater number of transitions were found in experiments,[19] the structures shown in Fig. 12 are not inconsistent with the experimental observations. Since there may not be any rational reasons why the correspondence between the computational prediction and the experimental result is not complete, it cannot be denied that the precision of the calculation is not sufficient or that the observed transitions result from small imperfections of the fabricated experimental apparatus.[6]

The radius ratio η is one of the significant parameters to determine the mode of Taylor vortex flow. It is fixed at 0.667 in the present study, and the bifurcation processes from the anomalous mode is presented. Cliffe *et al.*[8] reported that the

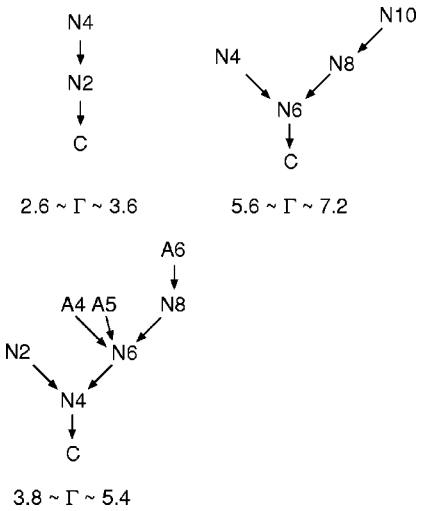

FIG. 12. Partial order structures representing transition processes to primary modes with two cells, four cells, and six cells. *C*: Couette flow, *Nn*: Normal *n*-cell mode; *An*: Anomalous *n*-cell mode.

anomalous mode loses its stability when the radius ratio is more than 0.83 and the gap is narrow. One of the extensions of the current work is the investigation of the time-dependent flows at large radius ratio.

IV. CONCLUSIONS

Taylor vortex flow between two concentric cylinders with moderate aspect ratios is investigated numerically. The mode formation processes are analyzed in detail. The end walls of the cylinders are stationary solid walls. The exchanges of flow pattern from the secondary modes to the primary modes are clarified qualitatively, and the Reynolds number at which the flow mode exchanges is determined. It is a novel evidence in this paper that a pair of counter-rotating cells disappears in the bifurcation processes from the normal secondary modes to the primary modes with a gradual decrease in the Reynolds number. The flow at the boundary between the two cells of the pair is inward. The present study showed the bifurcations asymmetric to the midplane in the axial direction, the bifurcations from the anomalous mode and the bifurcations which have an intermediate mode.

In the transient process from the flow in the anomalous mode, extra cells grow and merge into one vortex, and a saddle point appears in the working fluid. The merged cell has a flow from the outer to the inner cylinders near the end wall, and the flow mode becomes normal. As the merged vortex enlarges, the saddle point vanishes. Then, a pair of cells, which is adjacent to the merged cell and has a boundary with an inward radial flow between cells, disappears.

ACKNOWLEDGMENT

We are grateful to Dr. Y. Toya, Nagano National College of Technology, for several fruitful discussions.

[1] C. D. Andereck and F. Hayot, *Ordered and Turbulent Patterns in Taylor–Couette Flow* (Plenum, New York, 1992).
[2] C. B. Liao, S. J. Jane, and D. L. Young, "Numerical simulation of three-dimensional Couette–Taylor flows," Int. J. Numer. Methods Fluids **29**, 827 (1999).
[3] T. T. Lim, Y. T. Chew, and Q. Xiao, "A new flow regime in a Taylor–Couette flow," Phys. Fluids **10**, 3233 (1998).

[4]T. B. Benjamin, ''Bifurcation phenomena in steady flows in a viscous flow—II Experiment,'' Proc. R. Soc. London, Ser. A **359**, 27 (1979).
[5]P. Chossat and G. Iooss, *The Couette–Taylor Problem* (Springer-Verlag, Berlin, 1994).
[6]T. B. Benjamin and T. Mullin, ''Anomalous mode in the Taylor experiment,'' Proc. R. Soc. London, Ser. A **377**, 221 (1981).
[7]I. Nakamura and Y. Toya, ''Existence of extra vortex and twin vortex of anomalous mode in Taylor vortex flow with a small aspect ratio,'' Acta Mech. **117**, 33 (1996).
[8]K. A. Cliffe, J. J. Kobine, and T. Mullin, ''The role of anomalous modes in Taylor–Couette flow,'' Proc. R. Soc. London, Ser. A **439**, 341 (1992).
[9]D. K. Anson and K. A. Cliffe, ''A numerical investigation of the Schaeffer homotopy in the problem of Taylor–Couette flows,'' Proc. R. Soc. London, Ser. A **426**, 331 (1989).
[10]J. H. Bolstad and H. B. Keller, ''Computation of anomalous modes in the Taylor problem,'' J. Fluid Mech. **197**, 230 (1987).
[11]K. A. Cliffe, ''Numerical calculations of the primary-flow exchange process in the Taylor problem,'' J. Fluid Mech. **197**, 57 (1988).
[12]G. Pfister, H. Schmidt, K. A. Cliffe, and T. Mullin, ''Bifurcation phenomena in Taylor–Couette flow in a very short annulus,'' J. Fluid Mech. **191**, 1 (1988).
[13]K. S. Ball and B. Farouk, ''Bifurcation phenomena in Taylor–Couette flow with buoyancy effect,'' J. Fluid Mech. **197**, 479 (1988).
[14]D. Hirshfeld and D. C. Rapaport, ''Molecular dynamics simulation of Taylor–Couette vortex formation,'' Phys. Rev. Lett. **80**, 5337 (1998).
[15]D. C. Kuo and K. S. Ball, ''Taylor–Couette flow with buoyancy: Onset of spiral flow,'' Phys. Fluids **9**, 2872 (1997).
[16]M. Lücke, M. Mihelcic, and K. Wingerath, ''Front propagation and pattern formation of Taylor vortices growing into unstable circular Couette flow,'' Phys. Rev. A **31**, 396 (1985).
[17]G. P. Neitzel, ''Numerical computation of time-dependent Taylor-vortex flows in finite-length geometries,'' J. Fluid Mech. **141**, 51 (1984).
[18]Y. Takeda, K. Kobashi, and W. E. Fischer, ''Observation of the transient behavior of Taylor vortex flow between rotating concentric cylinders after sudden start,'' Exp. Fluids **9**, 317 (1990).
[19]I. Nakamura, Y. Toya, S. Yamashita, and Y. Ueki, ''An experiment on a Taylor vortex flow in a gap with a small aspect ratio (Bifurcation of flows in a symmetric system),'' JSME Int. J., Ser. II **33**, 685 (1990).
[20]C. A. Bieleck and E. L. Koschmieder, ''Taylor vortices in short fluid columns with large radius ratio,'' Phys. Fluids A **2**, 1557 (1990).
[21]T. Alziary de Roquefort and G. Grillaud, ''Computation of Taylor vortex flow by a transient implicit method,'' Comput. Fluids **6**, 259 (1978).
[22]D. Hirshfeld and D. C. Rapaport, ''Growth of Taylor-vortices: A molecular dynamics study,'' Phys. Rev. E **61**, R21 (2000).
[23]N. A. Hill, ''Numerical studies of side-by-side and other modes for the Taylor problem in a finite annulus,'' Comput. Fluids **16**, 445 (1988).
[24]C. F. Barenghi, ''Computations of transitions and Taylor vortices in temporally modulated Taylor–Couette flow,'' J. Comput. Phys. **95**, 175 (1991).
[25]C. L. Streett and M. Y. Hussaini, ''A numerical simulation of finite-length Taylor–Couette flow,'' in *Computational Fluid Dynamics*, edited by G. de Vahi Davis and C. Fletcher (Elsevier Science, New York, 1988).
[26]Y. Nishiura and D. Ueyama, ''A skeleton structure of self-replicating dynamics,'' Physica D **130**, 73 (1999).
[27]D. A. Anderson, J. C. Tannehill, and R. H. Pletcher, *Computational Fluid Mechanics and Heat Transfer* (Hemisphere, New York, 1984).
[28]T. Mullin, ''Mutations of steady cellular flows in the Taylor experiment,'' J. Fluid Mech. **121**, 207 (1982).
[29]E. L. Koschmieder, *Benard Cells and Taylor Vortices* (Cambridge University Press, Cambridge, MA, 1993).
[30]J. A. Cole, ''Taylor-vortex instability and annulus-length effect,'' J. Fluid Mech. **75**, 1 (1976).
[31]K. A. Cliffe and T. Mullin, ''A numerical and experimental study of anomalous modes in the Taylor experiment,'' J. Fluid Mech. **153**, 243 (1985).